Role of Dynamic Parameters of 18F-DOPA PET/CT in Pediatric Gliomas

Role of Dynamic Parameters of 18F-DOPA PET/CT in Pediatric Gliomas

Francesco Fiz 1, Fabiano Bini 2, Edoardo Gabriele 2, Gianluca Bottoni 1, Maria Luisa Garrè 3, Franco Marinozzi 2, Claudia Milanaccio 3, Antonio Verrico 3, Michela Massollo 1, Victoria Bosio 4, Marco Lattuada 4, Andrea Rossi 5, Antonia Ramaglia 5, Matteo Puntoni 6, Giovanni Morana, Arnoldo Piccardo 1

1From the Department of Nuclear Medicine, E.O. "Ospedali Galliera," Genoa.

2Department of Mechanical and Aerospace Engineering, "Sapienza" University of Rome, Rome.

3Neuro-oncology Unit, IRCCS Istituto Giannina Gaslini.

4Department of Anesthesiology, E.O. "Ospedali Galliera".

5Pediatric Neuroradiology Unit, IRCCS Istituto Giannina Gaslini, Genova.

6Clinical and Epidemiological Research Unit, University Hospital of Parma, Parma.

Abstract

Purpose of the Report

PET with 18F-DOPA can be used to evaluate grading and aggressiveness of pediatric cerebral gliomas. However, standard uptake parameters may underperform in circumscribed lesions and in diffuse pontine gliomas. In this study, we tested whether dynamic 18F-DOPA PET could overcome these limitations.

Patients and Methods

Patients with available dynamic 18F-DOPA PET were included retrospectively. Static parameters (tumor/striatum ratio [T/S] and tumor/cortex ratio [T/N]) and dynamic ones, calculated on the tumor time activity curve (TAC), including time-to-peak (TTP), slope steepness, the ratio between tumor and striatum TAC steepness (dynamic slope ratio [DSR]), and TAC shape (accumulation vs plateau), were evaluated as predictors of high/low grading (HG and LG) and of progression-free survival and overall survival.

Results

Fifteen patients were included; T/S, T/N, TTP, TAC slope steepness, and DSR were not significantly different between HG and LG. The accumulation TAC shape was more prevalent in the LG than in the HG group (75% vs 27%). On progression-free survival univariate analysis, TAC accumulation shape predicted longer survival ($P < 0.001$), whereas T/N and DSR showed borderline significance; on multivariate analyses, only TAC shape was retained ($P < 0.01$, Harrell C index, 0.93–0.95). On overall survival univariate analysis, T/N ($P < 0.05$), DSR ($P < 0.05$), and TAC "accumulating" shape predicted survival ($P < 0.001$); once more, only this last parameter was retained in the multivariate models ($P < 0.05$, Harrell C index, 0.86–0.89).

Conclusions

Dynamic 18F-DOPA PET analysis outperforms the static parameter evaluation in grading assessment and survival prediction. Evaluation of the curve shape is a simple-to-use parameter with strong predictive power.

Pediatric brain gliomas form a heterogeneous group of brain neoplasms that encompasses astrocytic and glioneuronal tumors, characterized by a circumscribed or diffusely infiltrating growth pattern, ranging from low grade to highly malignant.1–3 When compared with their adult counterparts, pediatric gliomas show divergent mechanisms of tumorigenesis, distinct molecular genetic alterations, and different clinical behavior (in particular low-grade gliomas, which differ substantially in the infrequency with which they transform to higher grade tumors), and are therefore considered biologically distinct entities.3–6

In the evaluation of pediatric brain gliomas, PET imaging with amino acid tracers has been demonstrated to overcome some limitations of conventional MRI, complementing advanced MRI techniques. In particular, 18F-labeled tracers have gained traction because of their longer half-life and superior spatial resolution when compared with the older 11C-based radiopharmaceuticals,7 which have led to their widespread use. One such tracer, 18F-dihydroxyphenylalanine (DOPA), has gained importance, given its versatility in pediatric oncology (brain gliomas8,9 and neuroblastoma10,11), and in nononcological conditions (congenital hyperinsulinism12). In particular, 18F-DOPA PET imaging in children with infiltrative gliomas correlates significantly with grade and outcome and, in diffuse midline gliomas, may determine the H3K27M mutation status noninvasively.13–15 Moreover, 18F-DOPA PET imaging is useful for biopsy planning and posttreatment monitoring, and can contribute to the stratification of patients with diffuse astrocytic tumors, thereby influencing their management8; 18F-DOPA PET might also provide relevant prognostic information in tumors that are not amenable to biopsy, such as diffuse intrinsic pontine gliomas (DIPGs).16

To date, the 18F-DOPA PET/CT analysis of pediatric brain gliomas has been based on standard static parameters such as tumor-to-striatum (T/S) and tumor-to-normal tissue (T/N) ratios.8 However, these parameters cannot evaluate certain lesion types reliably: circumscribed, low-

grade lesions may show marked tracer uptake because of their peculiar vascularization, whereas high-grade pontine diffuse lesions may exhibit faint tracer accumulation.

Dynamic parameters (ie, shape of time/activity curve, steepness of the intake slope, etc) might bridge this gap; however, they have never been tested in children. In newly diagnosed adult gliomas, few studies have so far investigated the role of dynamic 18F-DOPA PET/CT, without univocal results.17–21 Of note, given the known significant differences between pediatric and adult gliomas (underlined in the 2021 fifth edition of the World Health Organization [WHO] Classification of Tumors of the CNS),3 the conclusions drawn in these studies cannot be directly transferred to the pediatric population.

On the basis of these considerations, the overall objective of this retrospective study was to analyze whether dynamic 18F-DOPA PET/CT parameters can provide diagnostic and prognostic information in pediatric patients with brain gliomas. We also aimed to evaluate the degree of correlation between dynamic and static standard parameters.

PATIENTS AND METHODS

Patient Population

We retrospectively evaluated all consecutive pediatric patients (aged younger than 18 years on diagnosis) referred to our institutions between 2015 and 2019 for newly diagnosed treatment-naive (except biopsy) brain gliomas who had undergone conventional MRI and 18F-DOPA PET/CT (including static and dynamic acquisition), within 2 weeks of each other, and subsequent posttreatment MRI follow-up.

For each subject, the clinical information reviewed included the time of diagnosis, histology, molecular features, progression-free survival (PFS), and overall survival (OS). Progression-free survival and OS were defined as the interval between the initial diagnosis and the onset of disease progression and death from any cause.

Tumor grade was determined according to the 2021 WHO Classification of Tumors of the Central Nervous System.3 Surveillance was performed through regular clinical and MRI follow-up examinations; disease status was evaluated according to RAPNO (Response Assessment in Pediatric Neuro-Oncology) criteria.22–24

Ethics

A written informed consent form was signed by all patients' legal guardians, and patient assent was obtained when appropriate. The Regional Ethics Committee approved this retrospective study (R.P. 006/2019).

Image Acquisition

PET data acquisition was carried out by means of a PET/CT Discovery ST system (GE Healthcare, Milwaukee, WI). Participants fasted for at least 4 hours before 18F-DOPA administration (IASOdopa; IASON Labormedizin GmbH & Co. KG, Graz-Seiersberg, Austria); carbidopa premedication was never used. A low-dose CT scan, used for attenuation correction and localization of PET findings, was first carried out and was immediately followed by 30-minute 3D list-mode PET acquisition, initiated during the bolus injection of a median activity of 100 MBq (range, 74–185 MBq according to body weight). Static PET images were reconstructed with the list mode data acquired from 10 to 30 minutes postinjection,15,25 whereas dynamic PET images involved 6 consecutive frames of 20 seconds each, followed by 28 frames of 1 minute each.21,26 MRI studies were performed on a 1.5 T scanner (Intera Achieva; Philips, Best, the Netherlands) using an 8-channel head array receiving coil for sensitivity encoding parallel imaging. Each patient underwent routine clinical MRI scans, including precontrast axial spin echo T1-weighted images, fluid attenuation inversion recovery, and axial and coronal turbo spin echo T2-weighted images. After gadolinium compound bolus administration (0.1 mmol/kg, macrocyclic ionic agent), axial, coronal, and sagittal spin echo T1-weighted images were acquired along with an axial 3D T1-weighted sequence for neuronavigation purposes.

Image Analysis

Static images were analyzed on a dedicated workstation (OsiriX; Pixmeo SARL, Bernex, Switzerland), which also allowed post hoc coregistration of 18F-DOPA PET and MRI scans, as previously described.14 In detail, for each case, PET images were first visually inspected and the axial image slice that displayed the maximum tumor uptake was selected; whenever present, developmental venous anomalies were avoided27; a circular region of interest (ROI) of 8 mm diameter was manually drawn over the tumor (T) area that displayed the maximum uptake. In the event of negligible 18F-DOPA uptake, the ROI was placed in the center of the lesion.8,14

The radiotracer concentration in the ROI was normalized to the injected dose per patient body weight, and the SUVmax was obtained for each lesion (maximum pixel value [kBq/mL] within the ROI/injected dose [KBq]/patient weight [g]). Tumor uptake was normalized by means of 2 methods: by using the striatum uptake (S) and by drawing a large circular ROI (diameter 50 mm) in the normal cerebral hemisphere at the level of the centrum semiovale, including cortical and white matter (N). T/S and T/N ratios were thus calculated. Dynamic images were analyzed by means of the LIFEx software application (LITO; CEA, Inserm, CNRS, Université Paris-Saclay, Paris, France).28 The lesion was identified in the last phase of the dynamic PET

acquisition; morphological MRI was used as an anatomical reference. A volume of interest was generated semiautomatically by providing a “seeding point” and applying a thresholding algorithm (Nestle and Maisonobe); manual correction was then performed, whenever necessary. Once the volume of interest had been defined, a time activity curve (TAC) was generated with a specific LIFEX tool.

The shape of the TAC was visually analyzed and classified according to its trend (accumulating, stable, decreasing) by 2 readers (G.B. and F.F.), with a third expert reader (A.P.) being consulted whenever a consensus was needed.

The curve was then analyzed by means of the MatLab extension Grabit, which extracts the values of the single data points semiautomatically. Briefly, the user is asked to define the points of origin of the x and y axes on the TAC (TAC image and all the time points); the software output consists of the value of each time point. By plotting this value along with the time, the steepness of the slope of the curve and its time-to-peak (TTP) can be calculated. The slope steepness and the TTP were calculated by using the interval from the origin up to 30 minutes. The slopes were drawn on the lesions and on the striata of the patients; the ratio between the slopes of the lesion and the striata was defined as the dynamic slope ratio (DSR).

Statistical Analysis

Values of the variables are expressed as mean ± standard deviation. Comparison of the mean of continuous variables between groups was performed by applying the unpaired Student t test. The frequency of categorical variables in the groups was compared by means of Fisher exact test. The influence of single parameters on PFS or OS was tested by means of a univariate Kaplan-Meier model; specifically, thresholds of 1 and 1.6 were adopted for the T/S and T/N, respectively, as previously proposed,8,16 all other continuous variables were dichotomized. Furthermore, the impact of the clinical, static, and dynamic parameters was tested by applying a multivariate Cox regression model. Stata (version 13, Stata Corp) software was used for the analysis.

RESULTS

Characteristics of Patients and Lesions

During the study period, we evaluated 57 pediatric patients with suspected gliomas who had undergone 18F-DOPA PET/CT. Out of the initial population, 15 subjects (8 females; median age, 8 years; range, 3–16 years) were included in our study on the basis of the selection criteria (ie, ascertained pediatric glioma and 18F-DOPA PET/CT performed by means dynamic acquisition; see Fig. 1).

As 2 subjects with DIPGs did not undergo biopsy, their histological and molecular data were not available. Diagnosis was made on the basis of clinical and MRI criteria, in accordance with RAPNO guidelines.27

Overall, there were two grade 1 (1 ganglioglioma and 1 pilocytic astrocytoma), two grade 2 (1 diffuse astrocytoma, IDH-mutant and 1 diffuse astrocytoma, NOS), three grade 3 (diffuse pediatric-type high-grade glioma, H3-wildtype, and IDH-wildtype), and six grade 4 lesions (5 turned out to be diffuse midline gliomas, DMG, H3K27M-altered, and 1 diffuse pediatric-type high-grade glioma, H3-wildtype, and IDH-wildtype). The grade 3 and 4 tumors, as well as the 2 DIPGs that did not undergo biopsy, were classified as high-grade, whereas grade 1 and 2 lesions were classified as low-grade gliomas.

On brain MRI, 9 lesions displayed contrast enhancement, 5 of which exhibited signs of necrosis (ring-shaped enhancement). All brain tumors were positive on 18F-DOPA PET/CT (T/N > 1). Clinical features, 2021 WHO tumor characterization, and imaging characteristics of the patients are summarized in Table 1 and analytically detailed in Table 2.

Characteristics of the Uptake Curve

On visual analysis, the TACs showed 2 differently shaped patterns: constant “accumulation” type and “plateau” type. The former consisted of a rapid intake phase with subsequent further accumulation (ie, “accumulation curve”). In the latter case, after the first intake segment, the TAC became horizontal, without further significant variations (ie, “plateau curve”). We did not observe lesions with a “washout type curve,” that is, characterized by a tendency to decrease rapidly over time.

Of the 15 patients included in the analysis, 6 had an accumulation-type TAC and 9 had a plateau TAC. The plateau type was present in one grade 2 (diffuse astrocytoma, IDH-mutant), two grade 3 (diffuse pediatric-type high-grade glioma, H3-wildtype, and IDH-wildtype), and all grade 4 tumors (5 diffuse midline gliomas, H3K27-altered and 1 diffuse pediatric-type high-grade glioma, H3-wildtype, and IDH-wildtype) (Table 2).

Tumor Characterization Assessment

When evaluating all brain gliomas (low- and high-grade with a diffusely infiltrating growth pattern, and low-grade gliomas with a circumscribed growth pattern), the static parameters and most of the dynamic ones (tumor TAC slope steepness, TTP, and DSR) were not significantly different between low and high disease grades. Indeed, 3 of 4 low-grade lesions

(75%) showed an accumulating TAC shape, whereas this curve type was present in only 27% (3/11) of the high-grade lesions.

The target-to-background T/S and T/N values were not significantly different between lesions with pathological evidence of necrosis on MRI (ring enhancement) and those without. In this setting, the analysis of lesion slope steepness provided an excellent distinction between tumors with/without this characteristic, as the curve was much steeper in necrotic lesions than in nonnecrotic ones (0.17 ± 0.04 vs 0.076 ± 0.036, P = 0.0015).

Correlation Analysis and Multivariate Model Construction

On the Spearman matrix, DSR was significantly correlated with T/S median, T/N, and the slope of the tumor TAC. Moreover, T/S median and T/N were correlated with each other. Conversely, the TAC shape showed no correlation with any of the other parameters. These data are presented in the supplementary material (Supplemental Table 1, https://links.lww.com/CNM/A370). Consequently, for each outcome variable (PFS and OS), 2 models were constructed. In the "static" model, the clinical and pathology-related (age, sex, tumor grade, and contrast enhancement) variables were entered along with the uptake parameters from the equilibrium scan phase (T/S and T/N). In the dynamic mode, conversely, these 2 indices were replaced with DSR. Of note, the parameter "ring enhancement" could not be entered into any of the models, because it did not allow model convergence.

Progression-Free Survival

Eleven patients (73%) experienced disease progression; median PFS time was 9 months (range, 4–20 months).

On Kaplan-Meyer analysis, the curve shape (plateau vs accumulation) was able to distinguish PFS (P < 0.001), whereas T/N greater than 1.6 and the DSR showed borderline significance (P = 0.067 for both). T/S greater than 1 was not indicative of PFS (Figs. 2 and 3).

In a multivariate Cox regression model considering sex, age, grade, contrast enhancement, curve pattern, and DSR, the only parameter associated with PFS was the TAC shape (Harrell C index, 0.93) (Table 3). A second model, which included T/S and T/N instead of DSR (owing to collinearity), was therefore implemented. In this model, too, the only imaging parameter associated with PFS was TAC shape (Harrell C index, 0.95) (Table 4).

Overall Survival

After a median follow-up of 16 months (range, 6–37 months), all patients who had experienced disease progression died of disease.

Patients with OS below this median value had significantly higher T/S and T/N values than those who survived longer (1.87 ± 0.32 vs 0.94 ± 0.2, $P < 0.001$ and 2.16 ± 0.22 vs 1.19 ± 0.16, $P < 0.001$, respectively). In keeping with the case of PFS, patients showing a “plateau” shape of the 18F-DOPA time/activity curve had significant shorter OS than those with an “accumulation” pattern (12.4 ± 4.2 vs 26.8 ± 9.4, $P = 0.005$) (Fig. 2).

On Kaplan-Meyer analysis, T/N > 1.6, curve pattern and DSR were able to distinguish 2 groups with significantly different OS values. By contrast, T/S > 1 was not predictive (Fig. 4).

In a multivariate Cox regression model considering sex, age, grade, contrast enhancement, DSR, and TAC shape, only this last was significantly associated with OS (Harrell C index, 0.86) (Table 5).

A second model, which included T/S and T/N instead of DSR (owing to collinearity), was implemented. In this model, too, the only imaging parameter associated with OS was TAC shape (Harrell C index, 0.89) (Table 6).

DISCUSSION

The present study constitutes the first attempt to define the role of dynamic acquisition of 18F-DOPA PET/CT in the characterization of pediatric gliomas. Our data show that dynamic analysis can provide relevant information on tumor characterization and prognosis when DRS, curve slope, and TAC pattern are considered. Specifically, the analysis of TAC shape was able to identify patients at higher risk of disease progression and death. This subgroup was characterized by rapid tracer uptake in the first minutes of the acquisition, followed by a “plateau” pattern. By contrast, a more slowly rising uptake, with continuous “accumulation” during the whole observation period, was found in patients with longer survival. However, the pattern characterized by an early peak, followed by a steady decline, which is often reported in pediatric 18F-FET PET studies,29,30 was not observed in our series. Independently of the tracers used, these data suggest that the most aggressive tumors are characterized by a specific dynamic PET “signature”; this behavior is most likely multifactorial, depending on parameters such as transmembrane large amino acid transporter density, gene mutations, and cell proliferation.18,21,31 Furthermore, a potentially relevant factor in determining the curve shape could be the presence of blood-brain barrier disruption, which can facilitate influx to, but also efflux from, tumor lesions.21 In diffuse gliomas, blood-brain barrier damage is more common in high-grade tumors, thereby possibly explaining the evidence of tracer

washout from aggressive gliomas. As an additional finding, the slope of the dynamic 18F-DOPA curve was significantly steeper in lesions with radiological evidence of necrosis: this finding could be indicative of fast-growing tumors, in which the proliferating clone is not sufficiently supported by adequate neovascularization.32,33

Analysis of the curve pattern provided a more reliable prediction of the clinical outcome than the static uptake parameters. Indeed, both high-grade lesions and some low-grade ones, such as gangliogliomas and pilocytic astrocytomas, show high tracer avidity. However, this increased uptake is driven by different mechanisms: in high-grade tumors with an infiltrative pattern on MRI, rapid proliferation is associated with increased nutrient avidity; conversely, some low-grade lesions, which exhibit more circumscribed growth, may show increased vascularization with fenestrated epithelium, favoring a significant radiotracer uptake.34–36 Consequently, the mere evaluation of tumor uptake, as expressed by T/S and T/N, might be suboptimal in the estimation of biological aggressiveness when comparing pediatric gliomas that have different growth patterns (circumscribed vs diffuse). By contrast, observation of the trend in the uptake curve seems to provide more relevant information. Indeed, in our series, which included patients with different tumor growth patterns (both infiltrative and circumscribed), all but one patient showing a “plateau” curve experienced disease progression and died (on average, 6 and 12 months from the baseline, respectively), independently of the uptake ratio of the lesion. Of note, the only low-grade lesion that displayed a plateau-shaped curve was found in a patient with an IDH-mutant, adult-type diffuse astrocytoma, which can show a more aggressive behavior than its pediatric counterpart.

When considering the potential advantages of dynamic acquisition, it must be borne in mind that this scanning technique is relatively complicated and time-consuming, requiring significant expertise and, in younger children, a longer period of sedation. Moreover, performing dynamic acquisition can significantly reduce the machine throughput. In theory, interpretation of the output curve requires a certain mathematical expertise, or the availability of a specific software application (commercial or in-house), to extract the relevant curve parameters, such as curve slope and TTP. However, our analysis showed that merely observing the curve allowed us to classify tracer behavior into 2 broad categories, namely, accumulation and plateau. This qualitative observation proved to be the only independent predictor of PFS and OS.

A potential use of the uptake curve is the noninvasive biological characterization of intracranial lesions, which enables the reader to identify those that are at higher risk of rapid progression. This technique could be particularly valuable in cases in which biopsy is not routinely performed, such as in DIPG.37,38 In our series, visual analysis of the curve identified DIPG patients with an accumulating pattern, who experienced unusually long OS; conversely, those with a plateau-type curve displayed early progression and short OS. Further studies could investigate whether the curve pattern is associated with other therapy-relevant disease

hallmarks.39 In particular, the role of dynamic 18F-DOPA PET could be tested in the settings of pseudoprogression and pseudoresponse, which currently pose a relevant diagnostic challenge.9,40

This study presents a number of limitations. As it was a single-center, retrospective analysis, the sample was small and heterogeneous. However, the size of our sample was comparable to that of similar previous experiences,10,13–15,41 and its heterogeneity allowed us to gain potentially relevant insights into the characteristics of different types of pediatric gliomas. The curve slope and the TTP were obtained via a convoluted procedure involving a series of experimental software applications, which cannot easily be incorporated into clinical practice. However, we observed that the most relevant prognostic factor was the morphological pattern of the curve, which can be assessed visually immediately after acquisition, without the help of specific software tools.

CONCLUSIONS

Analysis of the dynamic 18F-DOPA PET curve pattern appears to be a promising noninvasive tool in the evaluation of pediatric cerebral gliomas, and can provide relevant complementary prognostic information.

REFERENCES

1. Sturm D, Pfister SM, Jones DTW. Pediatric gliomas: current concepts on diagnosis, biology, and clinical management. J Clin Oncol. 2017;35: 2370–2377.

2. Chen J, Dahiya SM. Update on circumscribed gliomas and glioneuronal tumors. Surg Pathol Clin. 2020;13:249–266.

3. Louis DN, Perry A, Wesseling P, et al. The 2021 WHO classification of tumors of the central nervous system: a summary. Neuro Oncol. 2021;23: 1231–1251.

4. Jones DT, Mulholland SA, Pearson DM, et al. Adult grade II diffuse astrocytomas are genetically distinct from and more aggressive than their paediatric counterparts. Acta Neuropathol. 2011;121:753–761.

5. Paugh BS, Qu C, Jones C, et al. Integrated molecular genetic profiling of pediatric high-grade gliomas reveals key differences with the adult disease. J Clin Oncol. 2010;28:3061–3068.

6. Chiang JC, Ellison DW. Molecular pathology of paediatric central nervous system tumours. J Pathol. 2017;241:159–172.
7. Conti M, Eriksson L. Physics of pure and non-pure positron emitters for PET: a review and a discussion. EJNMMI Phys. 2016;3:8.
8. Morana G, Piccardo A, Milanaccio C, et al. Value of 18 F-3,4-dihydroxyphenylalanine PET/MR image fusion in pediatric supratentorial infiltrative astrocytomas: a prospective pilot study. J Nucl Med. 2014;55:718–723.
9. Morana G, Piccardo A, Garrè ML, et al. Multimodal magnetic resonance imaging and 18 F-L-dihydroxyphenylalanine positron emission tomography in early characterization of pseudoresponse and nonenhancing tumor progression in a pediatric patient with malignant transformation of ganglioglioma treated with bevacizumab. J Clin Oncol. 2013;31:e1–e5.
10. Piccardo A, Morana G, Puntoni M, et al. Diagnosis, treatment response, and prognosis: the role of 18 F-DOPA PET/CT in children affected by neuroblastoma in comparison with 123 I-mIBG scan: the first prospective study. J Nucl Med. 2020;61:367–374.
11. Piccardo A, Puntoni M, Lopci E, et al. Prognostic value of 18 F-DOPA PET/CT at the time of recurrence in patients affected by neuroblastoma. Eur J Nucl Med Mol Imaging. 2014;41:1046–1056.
12. Ribeiro MJ, De Lonlay P, Delzescaux T, et al. Characterization of hyperinsulinism in infancy assessed with PET and 18 F-fluoro-L-DOPA. J Nucl Med. 2005;46:560–566.
13. Morana G, Piccardo A, Puntoni M, et al. Diagnostic and prognostic value of 18

F-DOPA PET and 1H-MR spectroscopy in pediatric supratentorial infiltrative gliomas: a comparative study. Neuro Oncol. 2015;17:1637–1647.

14. Morana G, Piccardo A, Tortora D, et al. Grading and outcome prediction of pediatric diffuse astrocytic tumors with diffusion and arterial spin labeling perfusion MRI in comparison with 18 F-DOPA PET. Eur J Nucl Med Mol Imaging. 2017;44:2084–2093.

15. Piccardo A, Tortora D, Mascelli S, et al. Advanced MR imaging and 18 F-DOPA PET characteristics of H3K27M-mutant and wild-type pediatric diffuse midline gliomas. Eur J Nucl Med Mol Imaging. 2019;46:1685–1694.

16. Morana G, Tortora D, Bottoni G, et al. Correlation of multimodal 18 F-DOPA PET and conventional MRI with treatment response and survival in children with diffuse intrinsic pontine gliomas. Theranostics. 2020;10:11881–11891.

17. Ponisio MR, McConathy JE, Dahiya SM, et al. Dynamic 18 F-FDOPA-PET/MRI for the preoperative evaluation of gliomas: correlation with stereotactic histopathology. Neurooncol Pract. 2020;7:656–667.

18. Nioche C, Soret M, Gontier E, et al. Evaluation of quantitative criteria for glioma grading with static and dynamic 18 F-FDopa PET/CT. Clin Nucl Med. 2013;38:81–87.

19. Chen W, Silverman DH, Delaloye S, et al. 18 F-FDOPA PET imaging of brain tumors: comparison study with 18 F-FDG PET and evaluation of diagnostic accuracy. J Nucl Med. 2006;47:904–911.

20. Schiepers C, Chen W, Cloughesy T, et al. 18

F-FDOPA kinetics in brain tu-
mors. J Nucl Med. 2007;48:1651–1661.
21. Ginet M, Zaragori T, Marie PY, et al. Integration of dynamic parameters in
the analysis of 18
F-FDopa PET imaging improves the prediction of molecular
features of gliomas. Eur J Nucl Med Mol Imaging. 2020;47:1381–1390.
22. Cooney TM, Cohen KJ, Guimaraes CV, et al. Response assessment in diffuse
intrinsic pontine glioma: recommendations from the Response Assessment
in Pediatric Neuro-Oncology (RAPNO) working group. Lancet Oncol.
2020;21:e330–e336.
23. Erker C, Tamrazi B, Poussaint TY, et al. Response assessment in paediatric
high-grade glioma: recommendations from the Response Assessment in Pe-
diatric Neuro-Oncology (RAPNO) working group. Lancet Oncol. 2020;21:
e317–e329.
24. Fangusaro J, Witt O, Hernáiz Driever P, et al. Response assessment in paedi-
atric low-grade glioma: recommendations from the Response Assessment in
Pediatric Neuro-Oncology (RAPNO) working group. Lancet Oncol. 2020;
21:e305–e316.
25. Law I, Albert NL, Arbizu J, et al. Joint EANM/EANO/RANO practice
guidelines/SNMMI procedure standards for imaging of gliomas using PET
with radiolabelled amino acids and [18
F]FDG: version 1.0. Eur J Nucl
Med Mol Imaging. 2019;46:540–557.
26. Kratochwil C, Combs SE, Leotta K, et al. Intra-individual comparison of
18
F-FET and 18
F-DOPA in PET imaging of recurrent brain tumors. Neuro
Oncol. 2014;16:434–440.
27. Morana G, Piccardo A, Garrè ML, et al. 18
F-DOPA uptake of developmental

venous anomalies in children with brain tumors. Clin Nucl Med. 2016;41:
e351–e352.
28. Nioche C, Orlhac F, Boughdad S, et al. LIFEx: a freeware for radiomic feature calculation in multimodality imaging to accelerate advances in the characterization of tumor heterogeneity. Cancer Res. 2018;78:4786–4789.
29. Dunkl V, Cleff C, Stoffels G, et al. The usefulness of dynamic O-(2-18
F-
fluoroethyl)-L-tyrosine PET in the clinical evaluation of brain tumors in children and adolescents. J Nucl Med. 2015;56:88–92.
30. Marner L, Lundemann M, Sehested A, et al. Diagnostic accuracy and clinical impact of [18
F]FET PET in childhood CNS tumors. Neuro Oncol. 2021;23:
2107–2116.
31. Fraioli F, Shankar A, Hyare H, et al. The use of multiparametric 18
F-fluoro-
L-3,4-dihydroxy-phenylalanine PET/MRI in post-therapy assessment of patients with gliomas. Nucl Med Commun. 2020;41:517–525.
32. Aldape K, Zadeh G, Mansouri S, et al. Glioblastoma: pathology, molecular mechanisms and markers. Acta Neuropathol. 2015;129:829–848.
33. Niida H, Takeuchi S, Tanaka R, et al. Angiogenesis in microvascular endothelial cells induced by glioma cells and inhibited by tumor necrosis factor
in vitro. Neurol Med Chir (Tokyo). 1995;35:209–214.
34. Puget S, Alshehri A, Beccaria K, et al. Pediatric infratentorial gangliogliomа.
Childs Nerv Syst. 2015;31:1707–1716.
35. Luo CB, Teng MM, Chen SS, et al. Intracranial gangliogliomа: CT and MRI findings. Kaohsiung J Med Sci. 1997;13:467–474.
36. Parenrengi MA, Aji YK. Multiple lesions accompanied by postoperative spontaneous intracystic hemorrhage in a pediatric patient with Pilocytic astrocytoma. Asian J Neurosurg. 2020;15:409–413.
37. El-Khouly FE, Veldhuijzen van Zanten SEM, Santa-Maria Lopez V, et al. Di-

agnostics and treatment of diffuse intrinsic pontine glioma: where do we stand? J Neurooncol. 2019;145:177–184.
38. Hoffman LM, Veldhuijzen van Zanten SEM, Colditz N, et al. Clinical, radiologic, pathologic, and molecular characteristics of long-term survivors of diffuse intrinsic pontine glioma (DIPG): a collaborative report from the international and European Society for Pediatric Oncology DIPG registries. J Clin Oncol. 2018;36:1963–1972.
39. Werbrouck C, Evangelista CCS, Lobón-Iglesias MJ, et al. TP53 pathway alterations drive radioresistance in diffuse intrinsic pontine gliomas (DIPG). Clin Cancer Res. 2019;25:6788–6800.
40. Bag AK, Wing MN, Sabin ND, et al. [11
C]-Methionine PET for identification of pediatric high-grade glioma recurrence. J Nucl Med. 2021;jnumed.120.261891.
41. Morana G, Puntoni M, Garrè ML, et al. Ability of (18)F-DOPA PET/CT and fused (18)F-DOPA PET/MRI to assess striatal involvement in paediatric glioma. Eur J Nucl Med Mol Imaging. 2016;43:1664–1672.

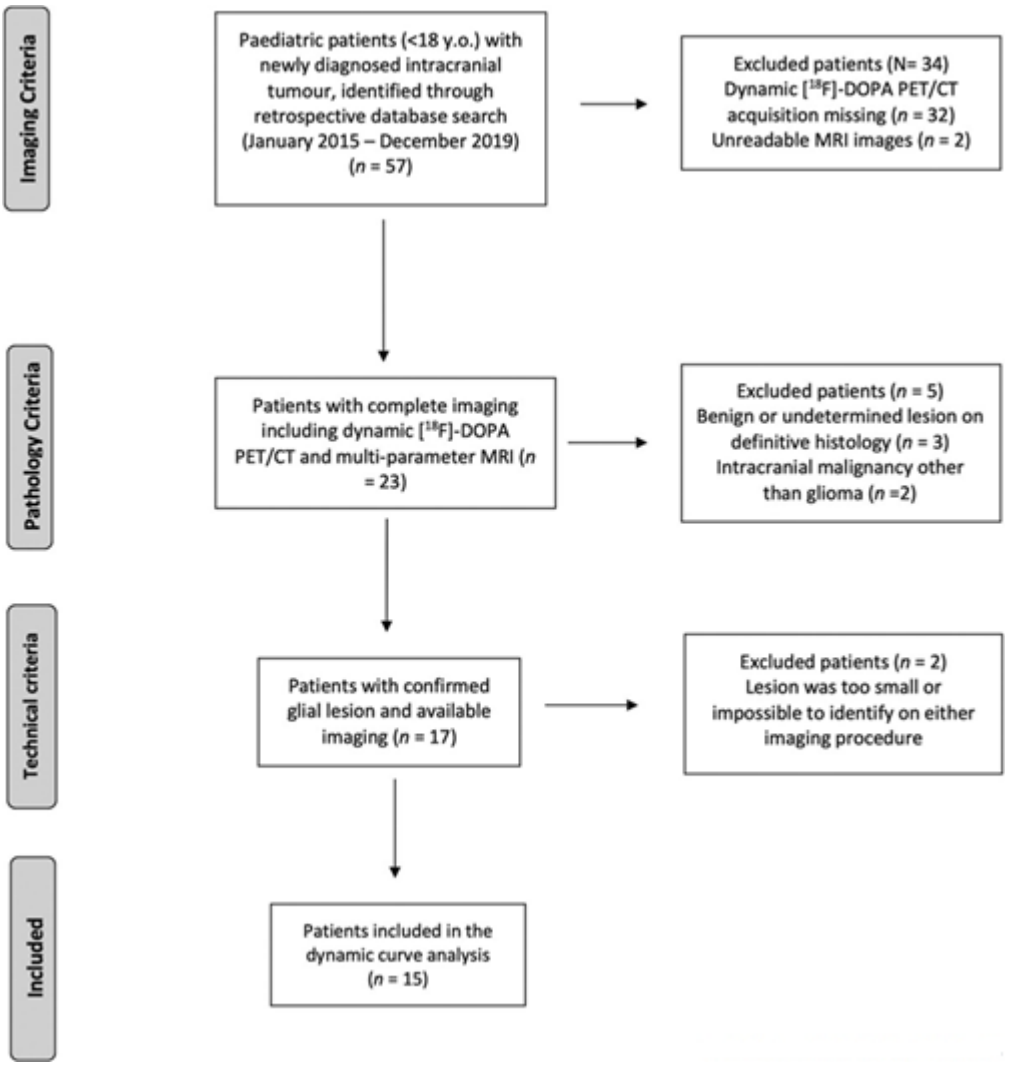

FIGURE 1. Patients' selection workflow.

Variable	Subjects Included (%)
Sex	
Female, n (%)	7 (46.6)
Male, n (%)	8 (53.4)
Age on diagnosis, median (range), y	8 (3–16)
<5 y, n (%)	5 (33.3)
≥5 y, n (%)	10 (66.6)
Classification of tumors	
Pilocytic astrocytoma	1 (6.6)
Ganglioglioma	1 (6.6)
Diffuse astrocytoma, NOS	1 (6.6)
Adult type–diffuse astrocytoma, IDH-mutant	1 (6.7)
Diffuse pediatric-type high-grade glioma, H3-wildtype, and IDH-wildtype	3 (19.8)
Diffuse pediatric-type high-grade glioma, H3-wildtype, and IDH-wildtype	1 (6.7)
Diffuse midline glioma, H3K27-altered	5 (33.3)
DIPG (clinical/radiological diagnosis)	2 (13.2)
Grade	
Grade 1, n (%)	2 (13.3)
Grade 2, n (%)	2 (13.3)
Grade 3, n (%)	3 (19.8)
Grade 4, n (%)	6 (40)
ND (DIPG)	2 (13.2)
^{18}F-DOPA uptake	
T/S ≤ 1 n (%)	5 (33)
T/S > 1 n (%)	10 (66)
^{18}F-DOPA curve	
Accumulation curve, n (%)	6 (40)
Plateau curve, n (%)	9 (60)
^{18}F-DOPA curve steepness	
Tumor curve slope steeper than that of striatum	7 (47%)
Tumor curve slope less steep than that of striatum	8 (53%)
Contrast enhancement	
Yes, n (%)	9 (60)
No, n (%)	6 (40)
Ring enhancement	
Yes, n (%)	5 (33)
No, n (%)	10 (66)

ND, not determined.

TABLE 1. Characteristics of the Study Cohort

Case	Sex	Age	Diagnosis	Who Grade	Location	MRI Necrotic Areas	MRI Contrast Enhancement	Curve Type
1	M	7	DIPG*	—	Pons	N	N	A
2	M	12	Diffuse midline glioma, H3K27-altered	4	L-DMJ	Y	Y	P
3	F	11	Ganglioglioma	1	L-DMJ	N	Y	A
4	F	6	Diffuse midline glioma, H3K27-altered	4	Pons	N	Y	P
5	M	10	Diffuse midline glioma, H3K27-altered	4	Pons	Y	Y	P
6	M	8	Diffuse pediatric-type high-grade glioma, H3-wildtype, and IDH-wildtype	4	R-Th	Y	Y	P
7	F	4	Diffuse midline glioma, H3K27-altered	4	R-Th/L-Th	Y	Y	P
8	M	15	Diffuse pediatric-type high-grade glioma, H3-wildtype, and IDH-wildtype	3	L-T, I, BG, Pa, CC	N	N	A
9	F	16	Diffuse pediatric-type high-grade glioma, H3-wildtype, and IDH-wildtype	3	L-F, Pa, T, CC	N	Y	P
10	M	8	Diffuse pediatric-type high-grade glioma, H3-wildtype, and IDH-wildtype	3	Pons	N	N	P
11	F	12	Diffuse midline glioma, H3K27-altered	4	Medulla	N	Y	P
12	F	7	Pilocytic astrocytoma	1	L-Th	Y	Y	A
13	F	4	DIPG*	/	Pons	N	N	A
14	M	3	Diffuse astrocytoma, NOS†	2	R-CER	N	N	A
15	F	14	Adult type–diffuse astrocytoma, IDH-mutant	2	R-F	N	N	P

M, male; F, female; N, no; Y, yes; L, left; R, right; DMJ, diencephalic mesencephalic junction; Th, thalamus; T, temporal; I, insular; F, frontal; BG, basal ganglia; Pa, Parietal; CC, corpus callosum; CER, cerebellar; A, accumulation; P, plateau.

*Histological and molecular data not available (biopsy not performed). Diagnosis made on the basis of clinical and MRI criteria in accordance with RAPNO guidelines.

†Molecular data not available.

TABLE 2. Detailed Demographics, WHO Grades, MRI Findings and 18 F-DOPA PET Curves

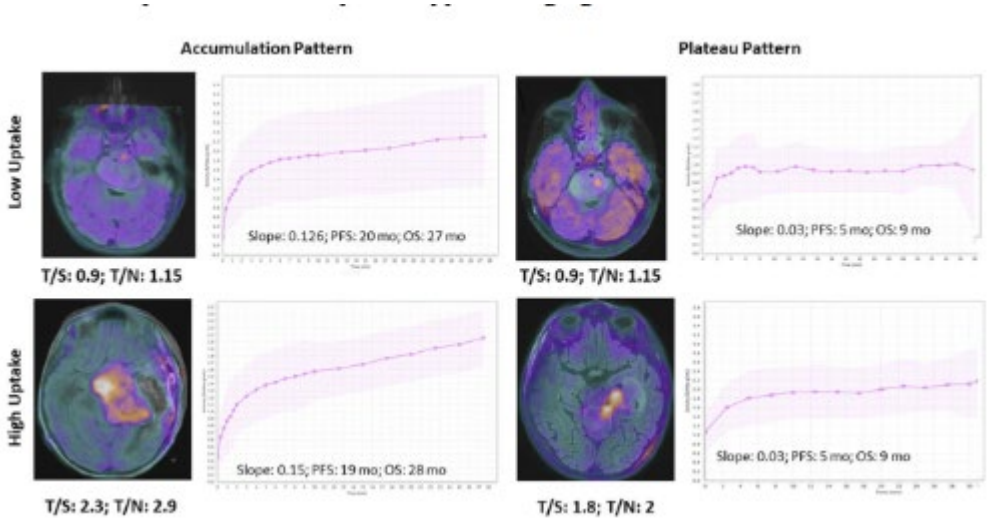

FIGURE 2. Comparison of OS and PFS across patients with high or low tracer uptake and with “accumulation” or “plateau” TAC

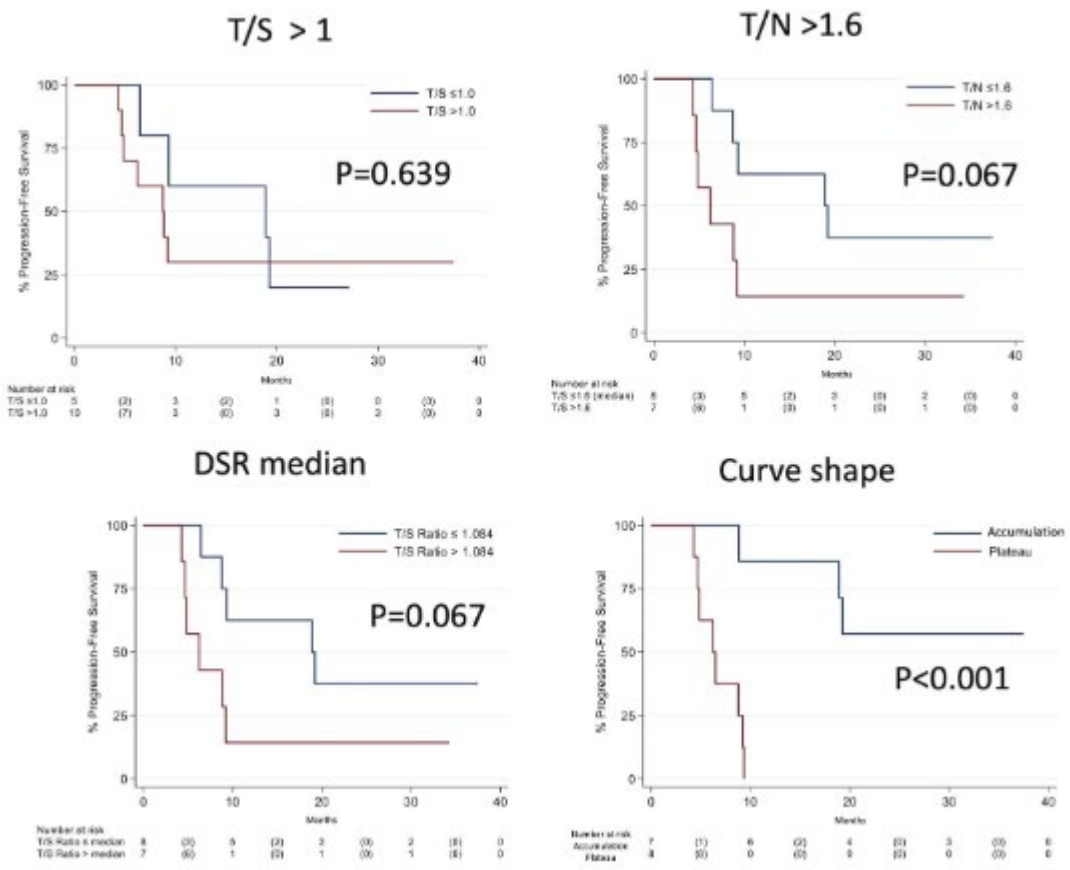

FIGURE 3. Progression-free survival by static and dynamic parameters

Parameter	HR	95% CI LB	95% CI UB	*P*
Sex	0.04	0.002	0.67	0.026
Age	1.13	0.88	1.44	0.319
Grade	0.9	0.69	1.17	0.458
CE	6.5	0.11	365.34	0.361
DSR	0.984	0.05	18.1	0.992
TAC shape	270	8	9038	0.002

HR, hazards ratio; CI, confidence intervals; LB, lower bound; UB, upper bound; CE, contrast enhancement.

TABLE 3. Multivariate PFS Model, Using the DSR

Parameter	HR	95% CI LB	95% CI UB	*P*
Sex	0.03	0.002	0.59	0.021
Age	1.35	0.88	2.1	0.162
Grade	0.89	0.66	1.19	0.456
CE	64	0.43	9516	0.102
T/S > 1	0.01	2.72^{-5}	4.8	0.147
T/N > 1.6	6.45	0.05	763	0.444
TAC shape	945	8.59	104,162	0.004

HR, hazards ratio; CI, confidence intervals; LB, lower bound; UB, upper bound; CE, contrast enhancement.

TABLE 4. Multivariate PFS Model, Using the Static Parameters

Parameter	HR	95% CI LB	95% CI UB	*P*
Sex	0.24	0.042	1.37	0.109
Age	1.03	0.82	1.29	0.761
Grade	0.95	0.723	1.26	0.757
CE	2.2	0.12	39.71	0.593
DSR	2.44	0.26	22.31	0.428
TAC shape	10.56	1.5	74.22	0.018

HR, hazards ratio; CI, confidence intervals; LB, lower bound; UB, upper bound; CE, contrast enhancement.

TABLE 5. Multivariate OS Model, Using the DSR

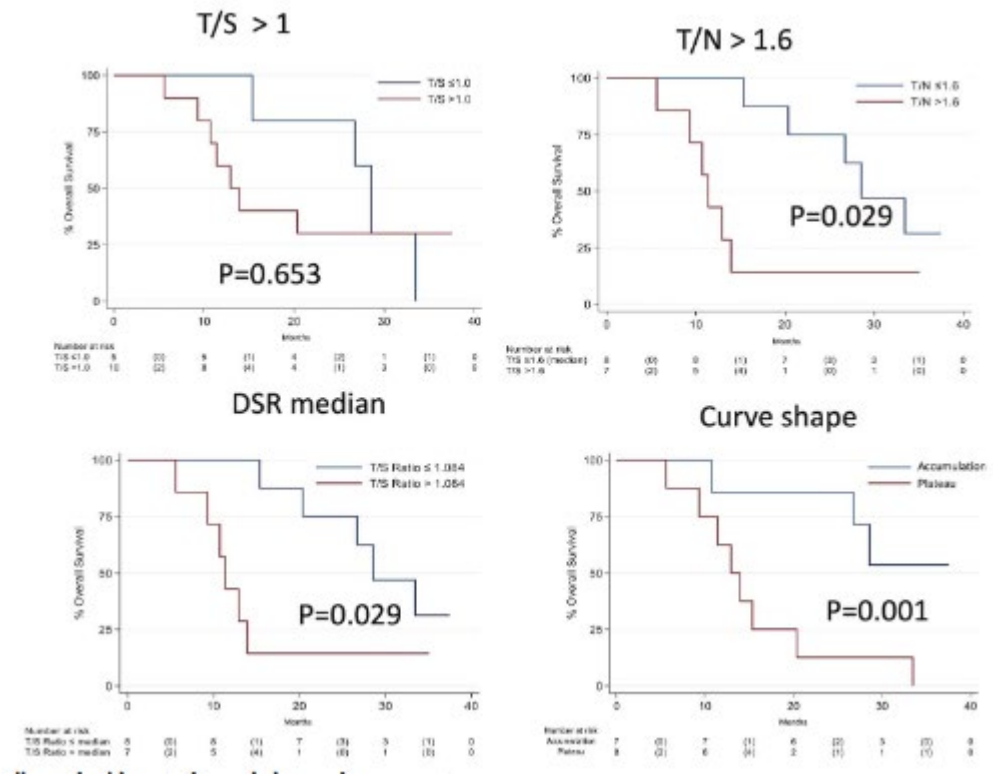

FIGURE 4. Overall survival by static and dynamic parameters

Parameter	HR	95% CI LB	95% CI UB	*P*
Sex	0.18	0.026	1.25	0.084
Age	1.1	0.83	1.45	0.489
Grade	1.01	0.76	1.34	0.13
CE	5.85	0.252	121	0.252
T/S > 1	0.12	0.005	2.97	0.196
T/N > 1.6	4.33	0.29	65.26	0.289
TAC shape	7.94	1.12	56.07	0.038

HR, hazards ratio; CI, confidence intervals; LB, lower bound; UB, upper bound; CE, contrast enhancement.

TABLE 6. Multivariate OS Model, Using the Static Parameters